View metadata, citation and similar papers at core.ac.uk
brought to you by CORE
provided by CiteSeerX

Proceedings of ESDA2006
8th Biennial ASME Conference on Engineering Systems Design and Analysis
July 4-7, 2006, Torino, Italy

ESDA2006-95386

VIBRATION SIGNATURE ANALYSIS OF REAL AND VIRTUAL DAMAGED GEARS

David Barbato, Michele Barsanti

Dipartimento di Matematica Applicata "U. Dini"– Università di Pisa
Via Bonanno Pisano 25/B – 56126 Pisa, Italy

Paola Forte, Salvatore Manconi, Gabriele Melani, Michele Vitali

Dipartimento di Ingegneria Meccanica, Nucleare e della Produzione – Università di Pisa
Via Diotisalvi 2 – 56126 Pisa, Italy

Maurizio Saroglia

AVIO S.p.A. Propulsione Aerospaziale
Via 1° Maggio 99 - 10040 Rivalta (To), Italy

ABSTRACT

A high performance rig designed to test gears (materials and geometries) in extreme load and speed conditions as in aerospace applications was used to test diagnostic systems by the only vibration analysis. The authors of the present report have implemented, in addition to some standard signal analysis techniques, some advanced methodologies (e.g. NA4, NB4), which are applied to the synchronously averaged signal to detect the smallest fault related variations in the tested gear vibration signature. The different techniques have been tested and compared on the signals of a gear that underwent failure, showing the good performance of the latter approaches compared to the more conventional ones.

A numerical simulation of the gear meshing was carried out to support the experimental campaign and the benchmarking of the diagnostic tools,. The stiffness computed by a FEM code was employed to simulate the gear system dynamic behavior with a lumped model, which was finally tuned using the experimental signals, to obtain indications on the crack evolution.

KEYWORDS: gears fault diagnostics, vibration monitoring, dynamic simulations

INTRODUCTION

Machine diagnostics consists in detecting failure pre-symptoms, so as to adopt suitable corrective actions to avoid the worst consequences of such a failure. The issue is particularly important for aircraft applications whose research reports are mainly focused on vibration monitoring techniques that can be classified according to the analysis domain into: a) frequency/cepstrum analysis [1, 2]; b) time/statistical analysis (time synchronous average, phase and amplitude demodulation of the meshing vibration [3], principal component analysis [4, 5]); c) time-frequency analysis (Wigner-Ville distribution [6-8], wavelet transform [9-11], instantaneous power spectrum [12]). Statistical measures of the residual signal (i.e. what remains of the synchronous signal averag after removing the regular gear meshing harmonics) such as the residual kurtosis (FM4), the quasi-normalized residual kurtosis (NA4) and the demodulated signal kurtosis (NB4) are actually considered good indicators for early gear crack detection [13]. Some vibration analysis methodologies applied to gear damage detection are reviewed and compared in [14, 15]. It is shown in [14] that an efficient and reliable diagnostic tool must integrate several techniques. In particular the spectral correlation density approach and the wavelet transform of the residual part of the time synchronous averaged signal appear to be very suitable to detect crack

Copyright © 2006 by ASME

Downloaded From: https://proceedings.asmedigitalcollection.asme.org on 06/29/2019 Terms of Use: http://www.asme.org/about-asme/terms-of-use

propagation in gears. The beta kurtosis and wavelet transform amplitude techniques implemented with the phase modulation of the time synchronous averaged signal are considered by some authors the most successful in gear fault diagnostics [15].

The "Research Center on Advanced Technology Mechanical Transmissions" (CRTM) of the University of Pisa has tested gears for aerospace applications. Since 2003 it is equipped with a high performance rig to carry out tests in extreme load and speed conditions. The bench has been used to test several diagnostic systems to detect various gear damage and failure modes, by means of vibration analysis [16,17]. More advanced diagnostic tools (e.g. NA4, NB4), in addition to standard diagnostic vibration indicators (RMS, Crest factor, Peak to Peak), have been tested offline to detect the smallest fault related variations of the vibration signature of the tested gear.

The experimental activity aimed at validating diagnostic methodologies can be particularly expensive in terms of time, if a defect is followed in its whole evolution from its initial growth to the gear failure. The same can be said for artificially faulted samples. A numerical simulation of the system dynamic behavior is surely a convenient means to perform preliminary testing of a diagnostic system, to support the interpretation of experimental results and to investigate a wider range of operating conditions and defects. A certain number of papers on mathematical models for the simulation of operating sound and faulty gears can be found in the literature (refer to [18] for a review). In particular it is worth to mention the work of Howard et al. [19, 20] where the variable tooth stiffness throughout the mesh cycle has been modeled using finite element analysis (FEA). The simulated phenomena include tooth cracking, spalling and the friction force effects at the meshing interface.

In this work a lumped model was developed on the basis of a FEA focused on meshing gear teeth stiffness. A tooth root crack was included. The gear system dynamic behavior was simulated taking into account the stiffness of both shaft and support and the mass of the various elements. The model was tuned using the experimental signals of a real gear with a known crack and different diagnostic techniques tested on the virtual test bench.

GEAR TEST RIG

The closed loop rig (Fig.1), designed and manufactured by RENK AG under AVIO specifications, is currently operating at CRTM and represents a further evolution of the "four square" concept. It is integrated within the CRTM test system, which consists of multiple lubrication subsystems and rig power control and monitoring subsystems.

In particular the test rig is made up of:

a) a 50 kW AC main motor; the speed is controlled via a vector AC drive;
b) a transmission "slave" gearbox both for speed multiplication and for loading by means of helicoidal gears one of which is moved by an electromechanical servo-actuator;
c) high speed quill shafts connecting the slave gearbox to the test articles (TA hereafter) gearbox;
d) a torque meter on one of the quill shafts;
e) an instrumented TA gearbox.

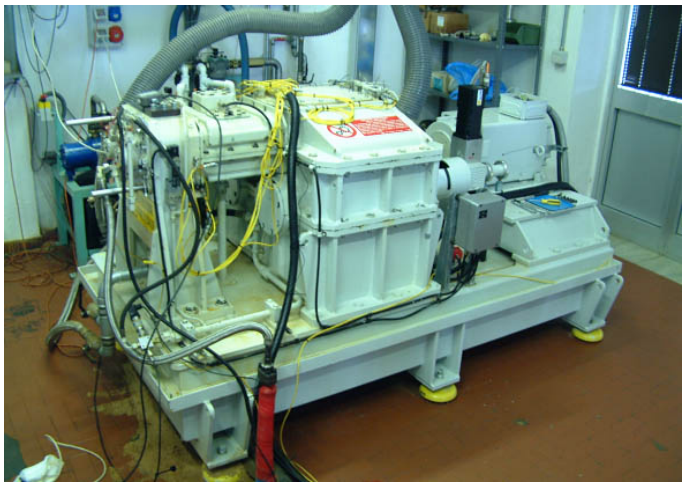

Figure 1: Gear test rig

The test rig can achieve the high performances reported in Tab.1.

Table 1: Rig main features

Maximum TA rotational speed	18000 rpm
Maximum continuous torque	500 Nm
Maximum TA oil temperature	180 °C

The whole transmission of the rig is mounted on roller bearings and is fully enclosed. To avoid contamination, the same synthetic aerospace oil (defined by the MIL-PRF-23699F specification) is used in the two independent lubrication circuits of the TA and slave gearboxes. The TA gears, presently object of experimental testing, are spur gears with 80 teeth.

CONTROL AND MONITORING

A control system was designed and implemented in LabView® to control angular speed, applied torque and temperature, thus making it possible to operate and control each test via a PC (Fig.2).

The monitoring system is able to detect at an early stage any damage that might appear, such as tooth fatigue cracking, pitting and scuffing. It is based on simple online processing of the signals generated by uniaxial high frequency accelerometers positioned on both the TA bearing supports (two for each) and by a triaxial accelerometer positioned on the main gear test rig housing.

Copyright © 2006 by ASME

Downloaded From: https://proceedings.asmedigitalcollection.asme.org on 06/29/2019 Terms of Use: http://www.asme.org/about-asme/terms-of-use

Signals from the various accelerometer sources are sampled at a frequency of 50 kHz; 4 channels, out of 11 available ones, are devoted to the acquisition of the signal from the 4 uniaxial accelerometers located near the TA. All data are recorded throughout the test; and a subsequent offline analysis is also possible. Some standard techniques both in the time domain and in the frequency domain have been implemented in the signal analysis.

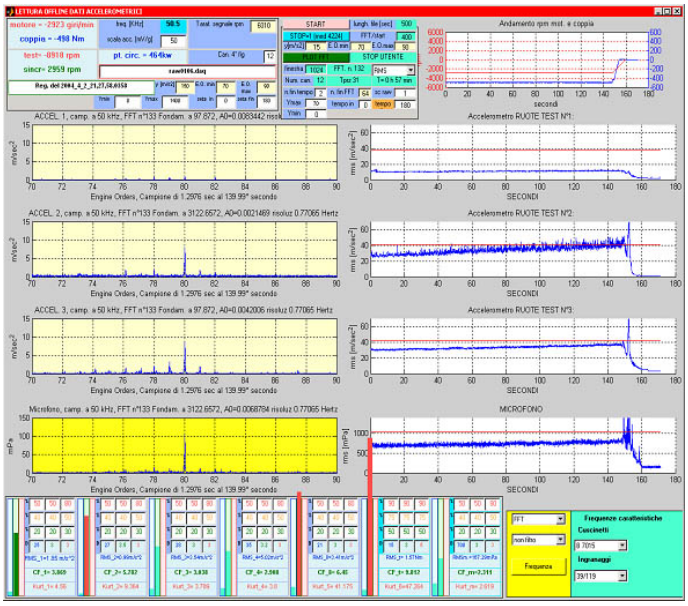

Figure 2: View of the control panel with FFT and CF values during a failure event.

At the present time, in the frequency domain, FFTs are simultaneously computed in real time for 4 channels. Generally, 3 channels are set to acquire accelerometer signals from the TA bearing housings while the fourth channel is switched to monitor other signals (torque, angular speed, vibrations in the slave gearbox, etc.).

As far as the time domain is concerned, RMS, Crest Factor (CF) and Kurtosis are computed on raw signals in real time for 6 channels. The processed values are used as alarm indicators by comparing them to previously defined thresholds.

Other techniques are based on the processing of signals sampled at constant frequency, but correlated with a tachometer signal indicating the time (s) corresponding to a gear known angular position.

During the experimental tests some gears underwent severe damage and in very few cases tooth rupture due to bending fatigue crack propagation. Figure 3 shows an example of a gear failure at the tooth root.

OFFLINE ANALYSIS OF A BENDING FAILURE EVENT

A set of numerical routines implementing some advanced methodologies for the detection of an incipient damage was used for an offline analysis of a single tooth bending failure. In this section, 9 methods will be compared: NA4, NA4*, NB4, NB4*, FM4, M6A, M8A, NP4 and $NP4_1$ (first order NP4) on the last 2400 s time interval of the fatigue bending test signals before shutdown.

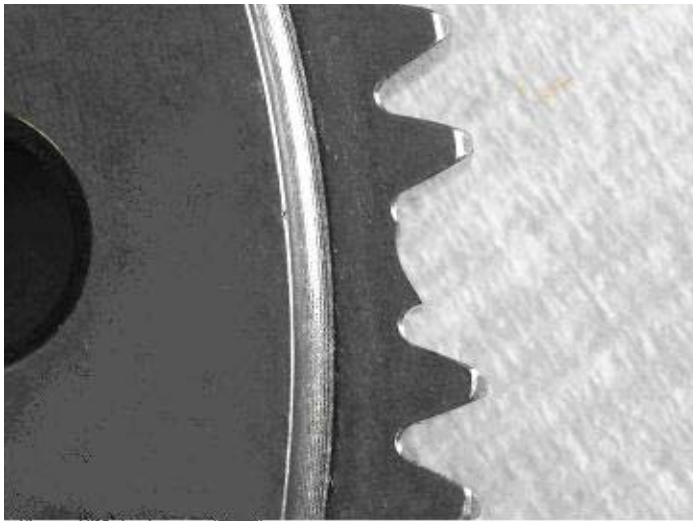

Figure 3: Bending stress failure

Before computing the various metrics, the raw acceleration signal was synchronously averaged to obtain the vibration signature using the algorithm presented in [17]. Time average was made over 1 s (119 gear rotations), and then the signal was resampled in order to obtain 640 samples for each turn. The rig angular speed was kept constant during the entire test run.

The origin of the time axis has been set at the instant corresponding to the online alarm that forced the rig shutdown. In order to compare the performance of the various failure indicators, and also for investigating the possibility of developing more efficient methods, we computed the time instants at which the 9 metrics would have issued an alert signal (yellow) and an alarm signal (red).

The threshold values for each metric were obtained considering their values on a time interval of 1000 s during which the gears were supposed to be in good conditions. On the same time interval, the maximum value M and the difference d between the maximum and the minimum values of the metric was computed.

The thresholds for the two alarm levels have been arbitrarily set to M+0.5d and M+d. The first instants at which the signal reaches each of the threshold values have been taken as alarm times, as it would happen in a real-time system. This provides a method for comparison only; it is not a criterion for optimal thresholds and alarm signaling in real time operating conditions.

A series of pictures showing the time evolution of different metrics is presented. The time interval is divided in three regions: green (no alarm), yellow (time between alert instant and alarm instant) and red (after alarm instant). The values of time instants indicate the moment at which alert and alarm

Copyright © 2006 by ASME

Downloaded From: https://proceedings.asmedigitalcollection.asme.org on 06/29/2019 Terms of Use: http://www.asme.org/about-asme/terms-of-use

would have been given with respect to the time of shutdown given by the conventional methods (RMS and CF on raw signal) actually implemented in the real-time control system.

NA4 parameter was computed using the following formula

$$NA4 = \frac{n\sum_{i=1}^{n}\left(r_i - \bar{r}\right)^4}{\left[\frac{1}{m}\sum_{j=1}^{m}\sum_{i=1}^{n}\left(r_{ij} - \bar{r}_j\right)^2\right]^2} \quad (1)$$

where r_i is the i-th sample of the residual signal (n=640 samples on each turn), $\bar{r}$ is the average of the residual signal on a single turn and m is the number of synchronous averages on which an average variance of the residual signal is computed. NA4* differs from NA4 only in the fact that, in the denominator, $\tilde{M}$ is the variance of the residual signal for gears in good conditions.

$$NA4^* = \frac{\frac{1}{n}\sum_{i=1}^{n}\left(r_i - \bar{r}\right)^4}{\left[\tilde{M}\right]^2} \quad (2)$$

In figures 4 and 5, the results of NA4 [21,22] and NA4* [23] analysis are shown.

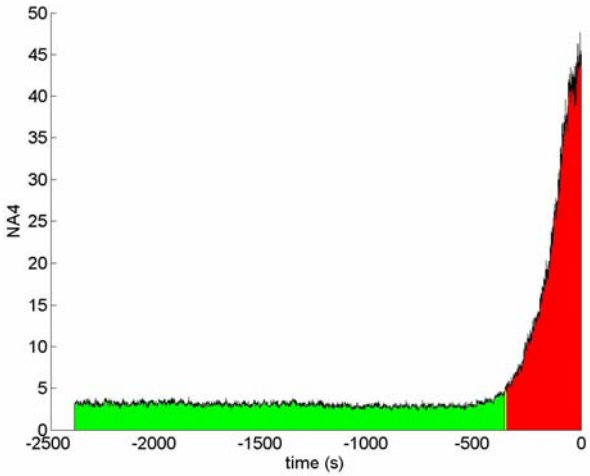

Figure 4: NA4 parameter. Alert would have given 360 s before rig shutdown, alarm 351 s before shutdown.

The ``locked'' denominator in NA4* (its value was computed at t=-2400 s, when the gear was supposed to be still in good conditions, and was kept fixed during all the investigated time interval) provides slightly better alarm times, and the trend after the alarm is more sharply defined than with NA4, due to the greatest range of NA4* values with respect to NA4 ones, that gives a less noisy signal. It is worth to notice that, in order to reduce the noise of NA4 signal, the length m of the average window for the computation of the denominator is 400 s.

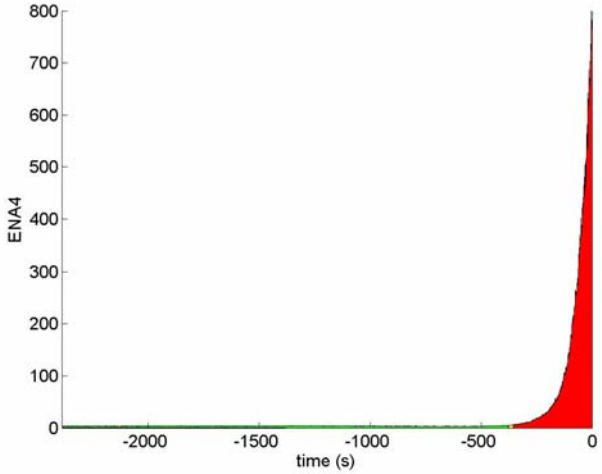

Figure 5: NA4* parameter. Alert would have given 377 s before rig shutdown, alarm 355 s before shutdown.

The parameter NB4 has been computed accordingly to the following formula:

$$NB4 = \frac{n\sum_{i=1}^{n}\left(E_i - \bar{E}\right)^4}{\left[\frac{1}{m}\sum_{j=1}^{m}\sum_{i=1}^{n}\left(E_{ij} - \bar{E}_j\right)^2\right]^2} \quad (3)$$

where E_i is the i-th sample of the envelope of the bandpassed signal (again n=640 samples on each turn), $\bar{E}$ is the average of the envelope of the bandpassed signal on a single turn and m is the number of synchronous averages on which an average variance of the envelope of the bandpassed signal is computed. NB4* differs form NB4 only for the fact that, in the denominator, $\tilde{T}$ is the variance of the envelope of the bandpassed signal for gears in good conditions.

$$NB4^* = \frac{\frac{1}{n}\sum_{i=1}^{n}\left(E_i - \bar{E}\right)^4}{\left[\tilde{T}\right]^2} \quad (4)$$

In figures 6 and 7 the NB4 and NB4* results are shown. They appear much noisier than NA4 and NA4*, and this is the main reason for their worse performance, according to the alarm criteria exposed in this section.

The NB4 signal clearly shows two regions with two different slopes in the last part of the test, even if the mechanical interpretation of this behavior is not evident. A longer time interval during which only the first level alarm was

Copyright © 2006 by ASME

Downloaded From: https://proceedings.asmedigitalcollection.asme.org on 06/29/2019 Terms of Use: http://www.asme.org/about-asme/terms-of-use

active is a symptom that these methods are not so sensitive to the damage increase as NA4 and NA4*.

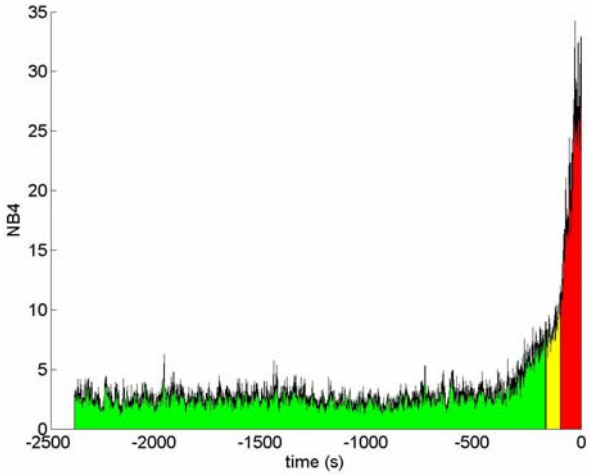

Figure 6 NB4 parameter. Alert would have given 197 s before rig shutdown, alarm 166 s before shutdown.

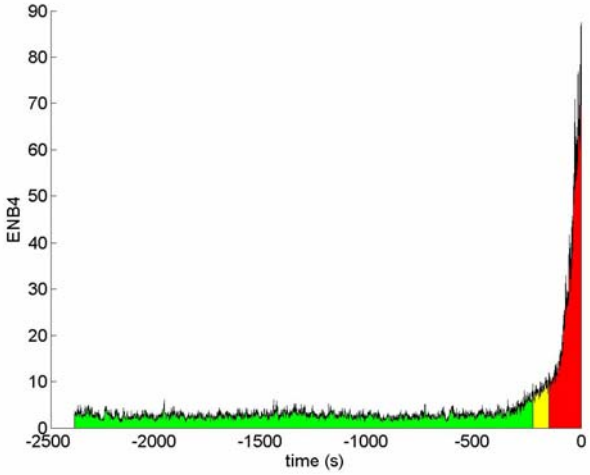

Figure 7: NB4* parameter. Alert would have given 227 s before rig shutdown, alarm 152 s before shutdown.

FM4 parameter [24] was computed using the following expression:

$$FM4 = \frac{n\sum_{i=1}^{n}\left(d_i - \bar{d}\right)^4}{\left[\sum_{i=1}^{n}\left(d_i - \bar{d}\right)^2\right]^2} \qquad (5)$$

where d_i is the i-th sample of the difference signal (n=640 samples on each turn) and $\bar{d}$ is the average of the difference signal on a single turn. In figure 8 the FM4 parameter is shown: a signal level change is evident as the failure initiated, but the metric does not provide a sharp indication of the damage increase, because the final values are less than twice the baseline value.

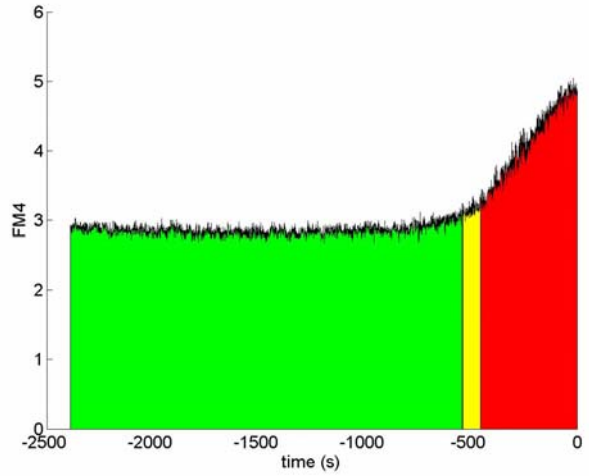

Figure 8: FM4 parameter. Alert would have given 539 s before rig shutdown, alarm 454 s before shutdown.

M6A and M8A parameters were computed according to:

$$M6A = \frac{n^2\sum_{i=1}^{n}\left(d_i - \bar{d}\right)^6}{\left[\sum_{i=1}^{n}\left(d_i - \bar{d}\right)^2\right]^3} \qquad (6)$$

$$M8A = \frac{n^3\sum_{i=1}^{n}\left(d_i - \bar{d}\right)^8}{\left[\sum_{i=1}^{n}\left(d_i - \bar{d}\right)^2\right]^4}. \qquad (7)$$

In figures 9 and 10, the results of the computation of M6A and M8A parameters are shown. Their alarm times are rather similar, but the time of first level alarm seems to be slightly worse than FM4 alarm time.

Lastly, figures 11 and 12 show the computation of NP4 parameter, developed according to [25]. This metric is obtained by an analysis of the Wigner-Ville transform; its enhanced first-order version $NP4_1$ analyzes the residual signal obtained removing the 1st order frequency component. The good result of $NP4_1$ method, using the alarm criterion of the first threshold overcoming, could be due to a random high value due to noise, thus increasing the probability of false alarm in real operating conditions. It is also evident that both signals do not increase monotonically after the alarm time, even if the signal level remains above threshold in both cases. This behavior makes these indicators unsuitable for following damage time evolution, and also for prognostic purposes.

Copyright © 2006 by ASME

Downloaded From: https://proceedings.asmedigitalcollection.asme.org on 06/29/2019 Terms of Use: http://www.asme.org/about-asme/terms-of-use

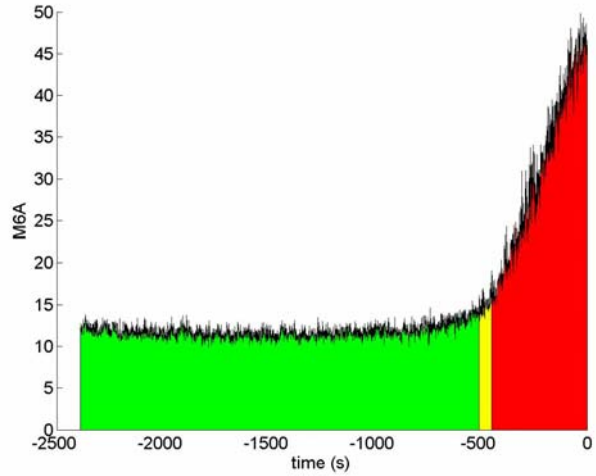

Figure 9: M6A parameter. Alert would have given 508 s before rig shutdown, alarm 450 s before shutdown.

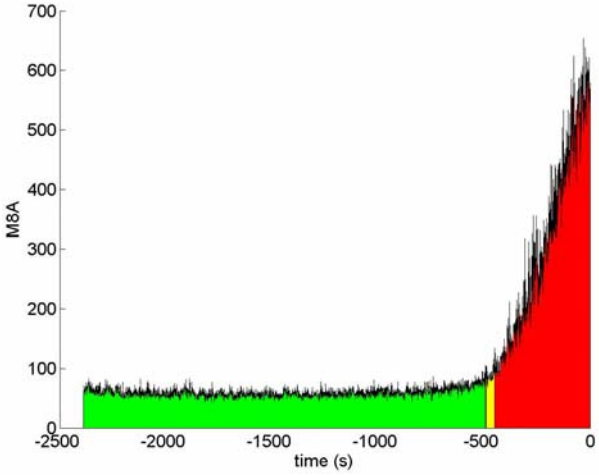

Figure 10: M8A parameter. Alert would have given 491 s before rig shutdown, alarm 450 s before shutdown.

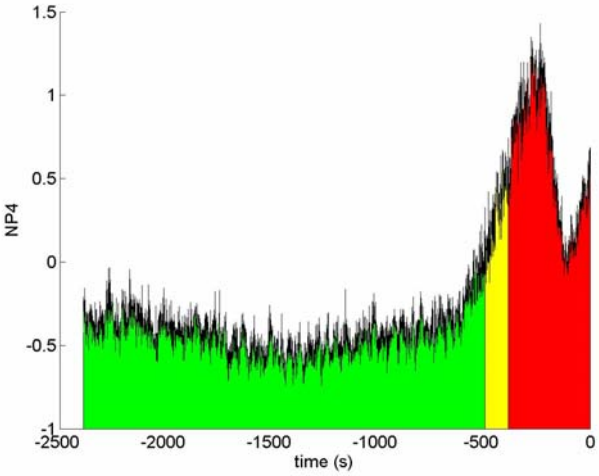

Figure 11: NP4 parameter. Alert would have given 495 s before rig shutdown, alarm 385 s before shutdown.

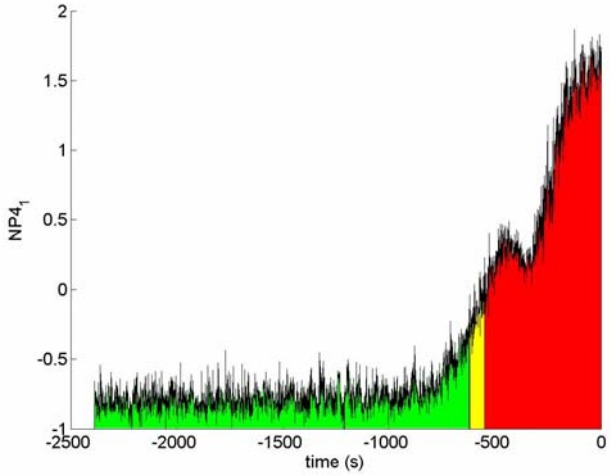

Figure 12: $NP4_1$ parameter. Alert would have given 620 s before rig shutdown, alarm 550 s before shutdown.

A summary of the alert and alarm times computed on synchronized signal using various methods is presented in Table 2.

Table 2: Alert and alarm times before rig shutdown

Method	Alert time (s)	Alarm time (s)
RMS	-183	-58
Kurtosis	-194	-69
NA4	-360	-351
NA4*	-377	-355
NB4	-197	-166
NB4*	-227	-152
FM4	-539	-454
M6A	-508	-450
M8A	-491	-450
NP4	-495	-385
$NP4_1$	-620	-550

THE LUMPED MODEL

A lumped dynamic model was developed to approximately represent the dynamic behavior of the described test bench.

First a 2D finite element (FE) model of the gears (in plane strain) was developed (Fig.13), with the aim of computing the gear stiffness variation in meshing due to tooth contact and bending (static and dynamic friction effects were neglected for simplicity sake), as function of the gear angular position; stiffness was calculated by determining the gear relative angular displacement due to a given applied torque for different gear angular positions.

The so calculated meshing stiffness is a periodic function of the rotation angle, the period being the angular span of a tooth since every tooth has the same stiffness. Moreover the stiffness appears not load independent, therefore in the FEA the

Copyright © 2006 by ASME

Downloaded From: https://proceedings.asmedigitalcollection.asme.org on 06/29/2019 Terms of Use: http://www.asme.org/about-asme/terms-of-use

simulated load (driving torque applied to the pinion) has the same value of the real one applied to the test rig.

Secondly the effects of defects, consisting mainly in cracks of different shape and length at the tooth root, were included in the model by means of a modified stiffness function. An increased crack length causes a decrease in the meshing stiffness when the cracked tooth is close to the meshing zone. That brings a discontinuity in the periodicity of the meshing stiffness.

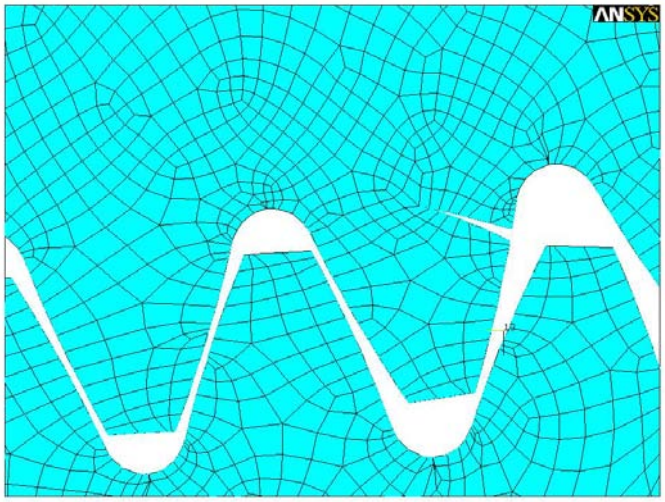

Figure 13: FEM model of the meshing gear sectors with a central cracked tooth.

Furthermore, a simplified model of the test rig was developed in the Simulink environment; such a model is made of two bodies representing the two mating wheels and their shafts. They are connected to the housing by bearings where the accelerometers are located. To take into account the housing influence on the accelerometer signal, besides the conventional bearing stiffness and damping parameters, K_x and C_x, an additional lumped mass m_s was considered.

The inertia characteristics m_i and J_i of the i-th wheel, including its shaft, were calculated by means of a 3D solid modeling software.

The two wheels are connected by a compliant link simulating the previously calculated meshing stiffness K_t as function of the rotation angle θ_1 directed as the gear line-of-action.

Therefore the dynamic model is a plane model (Fig.14), i.e. it considers plane gears, and has 4 d.o.f., the rotating motion of the two wheels and the translatory motion of each body in the direction parallel to the gear line-of-action. In the test rig the accelerometers are mounted on the bearing housings and oriented in such a direction, therefore it is possible to compare the experimental accelerometer signal with the simulated one.

A driving torque equal to the experimental one is applied to the pinion, while a resistant torque proportional to the square of the angular speed is applied to the driven wheel. Working on the load proportionality coefficient c one can obtain a steady speed value equal to the experimental one (i.e. ω = 1351 rad/s).

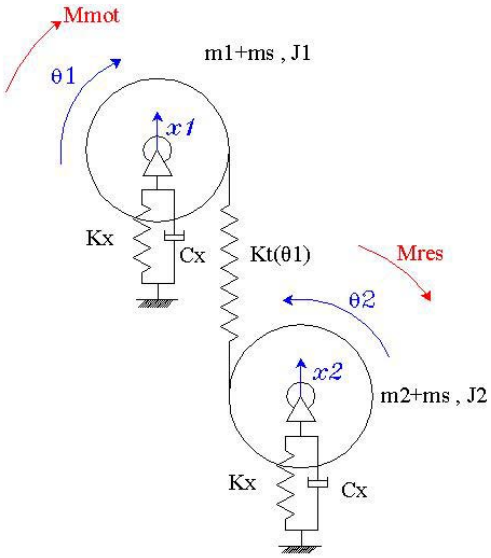

Figure 14: 4 DOF model of test rig.

Therefore the equations describing the dynamic equilibrium are the following:

$$\begin{cases} J_1\ddot{\theta}_1 + K_t r^2(\theta_1-\theta_2) + K_t r(x_2-x_1) = M_{mot} \\ J_2\ddot{\theta}_2 + K_t r^2(\theta_2-\theta_1) + K_t r(x_1-x_2) = -c\dot{\theta}_2^2 \\ (m_1+m_s)\ddot{x}_1 + K_x x_1 + K_t(x_1-x_2) + K_t r(\theta_2-\theta_1) + c_x\dot{x}_1 = 0 \\ (m_2+m_s)\ddot{x}_2 + K_x x_2 + K_t(x_2-x_1) + K_t r(\theta_1-\theta_2) + c_x\dot{x}_2 = 0 \end{cases} \quad (8)$$

MODEL TUNING AND VALIDATION

The simulations provide the plot of various quantities as function of time; in particular it is interesting to study the pattern of the acceleration signal at the shaft bearings ($\ddot{x}_1$) to compare it with the experimental accelerometer signal.

In order to do that, it is necessary to determine the meshing stiffness K_t as function of θ_1 for a gear with a crack identical to the experimental one. The crack profile was identified with adequate approximation by processing photographs of the cracked tooth (Fig.3). Such a profile was then included in the FE model, considering different crack lengths and thus calculating the corresponding meshing stiffness. The latter were then used in the lumped parameter model.

Such a comparison makes it possible to tune the model since some parameters are unknown (i.e. K_x, C_x., and m_s); so it is necessary to minimize the difference between simulated and experimental results carrying out a few simulations with different parameter values until a satisfactory configuration is found. The model tuning must be carried out for a known crack condition. In particular, the FFT spectra of experimental and

Copyright © 2006 by ASME

Downloaded From: https://proceedings.asmedigitalcollection.asme.org on 06/29/2019 Terms of Use: http://www.asme.org/about-asme/terms-of-use

simulated acceleration signals of the faultless gear were compared for tuning, and model parameters modified, until the amplitudes of the most significant peaks were the same for the two signals (Fig.15). The attention was focused on a peak related to a traslatory mode, at 678 Hz, a peak related to a torsional mode, at 2380 Hz, and a peak related to the meshing frequency, at 17200 Hz, corresponding to the 80th shaft order. The third significant peak of the experimental signal, corresponding to the 39th shaft order, does not appear in the simulated signal but it is typical of the test-rig due to the meshing of the transmission slave gears not included in the model.

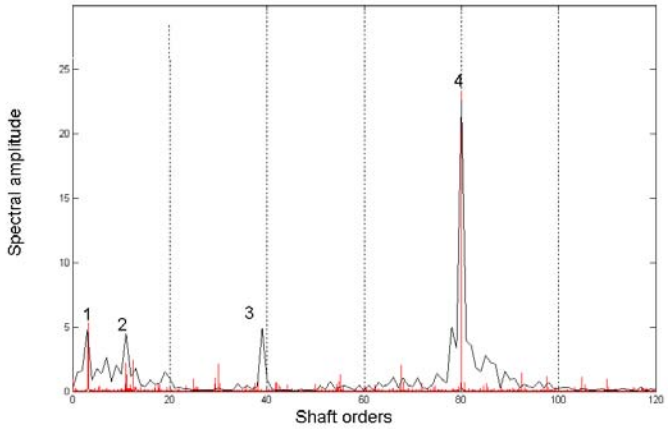

Figure 15: Comparison of experimental FFT (black line) and simulated FFT (red line) after model tuning.

The RMS evaluation of the simulated signal makes it possible to compare the latter with the experimental one on the basis of the same parameter; Tab.3 summarizes the RMS values of the experimental and simulated acceleration signals in the case of the faultless tooth. For the experimental signal we consider the first processed data (synchronous average) as those of a presumably faultless gear.

Table 3: RMS values of faultless gear

Experimental RMS	0,1418
Simulated RMS	0,1456

The crack evolution in time was estimated on the basis of Paris' law:

$$\frac{da}{dN} = C\Delta K^{m} \qquad (9)$$

where the first term represents the crack growth rate expressed in [mm/cycle], ΔK is the stress intensity factor range expressed in [MPa$\sqrt{m}$], while *m* and *C* are two parameters that depend on the material properties and on test conditions.

The cracked tooth was considered as a cracked beam subjected to bending. The bending moment applied to the cracked tooth was evaluated considering a particular angular position of the gears. (the one with the maximum load on the cracked tooth). Since the teeth in contact act as springs in parallel they share the load proportionally to their stiffness.

Modified load sharing due to the decreased stiffness of the cracked tooth was taken into account in the estimation of the cycles corresponding to crack propagation. The lower load causes an increase of the fatigue crack growth cycles.

Since experimental crack length data and corresponding growth cycles were not available, the Paris' law coefficients, *m* and *C* were tuned on the basis of the experimental RMS acceleration signal time evolution. The previously tuned Simulink model was used to simulate the acceleration signal of gears with progressive cracks and calculate the corresponding RMS values. Estimating the crack evolution with Paris' Law it is possible to associate estimated cycles to simulated RMS acceleration values making it possible to compare on a time scale the experimental and simulated RMS patterns. Finally, "equivalent" Paris' coefficients (for the 2D model) were determined by curve fitting. The results are shown in Fig.16 where the red line represents the experimental RMS acceleration signal plotted versus time while the black dots are the simulation RMS values for different crack lengths (from 0 to 1 mm).

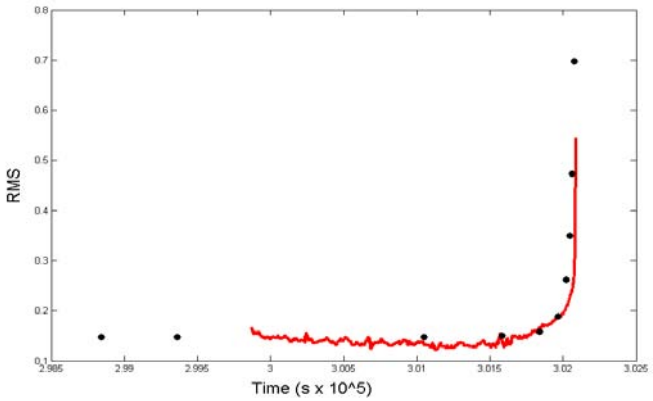

Figure 16: Comparison of experimental RMS acceleration signal time evolution (red line) with RMS values of simulated signal (black dots) calculated on the basis of Paris' law.

The FFT spectrum of the tuned model virtual signal was finally compared with that of the synchronously averaged experimental signal. Figures 17 and 18 represent the spectrograms of the simulated and experimental signals.

The experimental plot has many more peaks due to the fact that the numerical model has a reduced number of d.o.f. that cannot highlight all the dynamic characteristics of the real system. This limitation of the model is particularly evident if one compares the two FFTs referred to the last analyzed crack length before failure (estimated around 0.7mm) (Fig.19) because the highest peaks in the experimental spectrum are

Copyright © 2006 by ASME

Downloaded From: https://proceedings.asmedigitalcollection.asme.org on 06/29/2019 Terms of Use: http://www.asme.org/about-asme/terms-of-use

related to frequencies and modes that are not visible in the simulation.

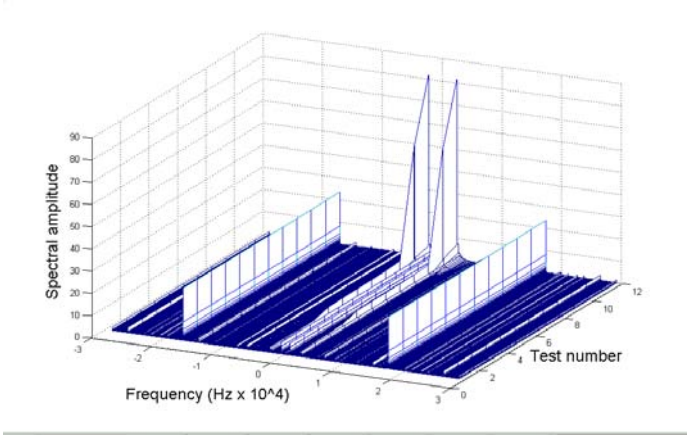

Figure 17: Spectrogram of the simulated accelerometer signal.

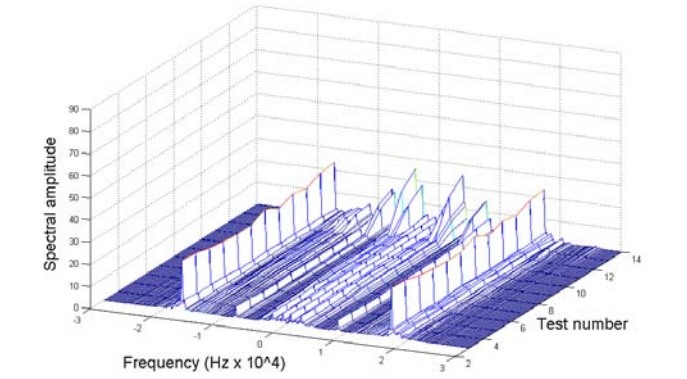

Figure 18: Spectrogram of the experimental averaged accelerometer signal.

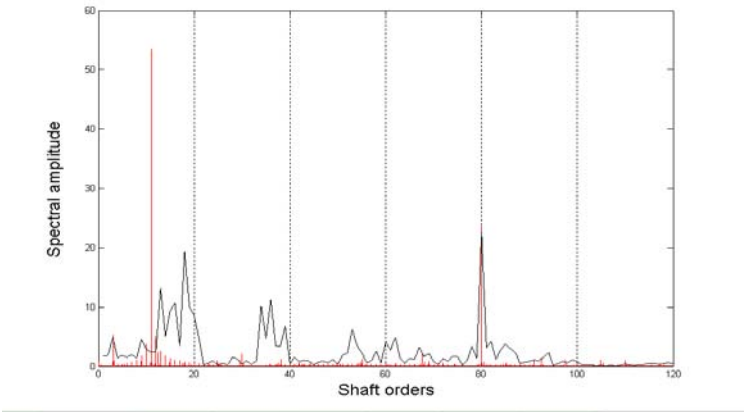

Figure 19: Comparison of experimental FFT (black line) and simulated FFT (red line) near tooth failure.

Moreover as the crack grows and the RMS value increases the simulated FFT peaks are much higher than the experimental ones because the model is tuned to have the same RMS value of the real system but has less vibration modes, due to the low number of d.o.f. of the model, to make up that value.

Nonetheless some typical aspects of the acceleration signals of faulted gears can be observed such as the rise of sidebands about the carrier frequency that in the simulation case is the typical torsional mode frequency (2380 Hz).

CONCLUSIONS

Some advanced diagnostic methodologies have been tested and compared on the acceleration signals of a gear that underwent failure, showing the good performance of these approaches compared to the more conventional methods. In particular, in the analized case, $NP4_1$ proved to be the most effective and prompt technique in early tooth bending fatigue failure detection.

To support the experimental campaign and the benchmarking of the diagnostic tools, a numerical simulation of the gear meshing was carried out with a simplified dynamic model, which was tuned using the experimental signals. Such a model could be a useful aid to estimate the time evolution of the averaged signal RMS value and to evaluate a priori the growth time of a specific crack for different operating conditions and most of all the trend of the acceleration signals and its related parameters. On these bases it will be possible to elaborate diagnostic (and eventually prompt maintenance) strategies before catastrophic crack propagation takes place.

A more complex (3D) dynamic model including out-of-plane vibration modes should be developed to obtain a better agreement with the experimental signal and greater simulation reliability.

ACKNOWLEDGMENTS

The authors thank Mr Gianni Ferioli for his fundamental contribution in data acquisition and data base maintenance and Dr Gregorio Guidi for his help in the computation of NASA parameters.

REFERENCES

[1] Randall R., 1980, *Advances in the application of cepstrum analysis to gearbox diagnostics*, 2nd International Coference of Vibration in Rotating Machinery, Cambridge, U.K., 169-174.

[2] Rubin R., Sidahmed M., 1997, *Diagnostics of gear systems using the Spectral Correlation Density of the vibration signal*, Proc. Symposium on Fault Detection, Supervision and Safety for Technical Processes, Hall UK, 977-982.

[3] McFadden P.D., 1986, *Detecting fatigue cracks in gears by amplitude and phase demodulation of the meshing vibration*, Journal of Vibration, Acoustics, Stress, and Reliability in Design, 108, 165-170.

[4] Baydar N., Chen Q., Ball A., Kruger U., 2001, *Detection of incipient tooth defect in helical gears using multivariate statistics*, Mechanical Sistems and Signal Processing, 15(2), 303-321.

Copyright © 2006 by ASME

Downloaded From: https://proceedings.asmedigitalcollection.asme.org on 06/29/2019 Terms of Use: http://www.asme.org/about-asme/terms-of-use

[5] Li W., Shi T., Liao G., Yang S., 2003, *Feature extraction and classification of gear faults using principal component analysis*, Journal of Quality in Maintenance Engineering, 9(2), 132-143.
[6] Choy F.K. et al., 1996, Vibration signature analysis of a faulted gear system, Propul.Power, 12(2),289-295.
[7] Staszewski W.J., Tomlison G.R., 1997, *Time-frequency analysis in gearbox fault detection using the Wigner-Ville distribution and pattern recognition*, Mechanical Sistems and Signal Processing, 11, 673-692.
[8] Baydar N., Ball A., 2001, *A comparative study of acoustic and vibration signals in detection of gear failures using*, Mechanical Sistems and Signal Processing, 15(6), 1091-1107.
[9] Staszewski W.J., Tomlison G.R., 1994, *Application of the wavelet transform to fault detection in spur gear,* Mechanical Sistems and Signal Processing, 8, 289-307.
[10] Wang W.J., Mc Fadden P.D., 1996, *Application of wavelets to gear box vibration signals for fault detection*, Journal of Sound and Vibration, 192, 927-937.
[11] Baydar N., Ball A., 2003, *Detection of gear failures via vibration and acoustic signals using wavelet transform*, Mechanical Sistems and Signal Processing, 17(4), 787-804.
[12] Yesilyurt I.,2003, *Fault detection and location in gears by the smoothed instantaneous power spectrum distribution*, NDT & E International, 36(7), 535-542.
[13] Choy F.K. et al., 1994, *Vibration signature analysis of a faulted gear transmission system*, NASA Technical Memorandum 106623.
[14] Dalpiaz G., Rivola A., Rubini R., 2000, *Effectiveness and sensitivity of vibration processing techniques for local fault detection in gears*, Mechanical Systems and Signal Processing, 14(3), 387-412.
[15] Wang W.Q., Ismail F., Golnaraghi M.F., 2001, *Assessment of gear damage monitoring techniques using vibration measurements*, Mechanical Systems and Signal Processing, 15(5), 905-922.
[16] Amorena M., Barsanti M., Gubinelli M., Guzzo F., Manfredi E., Plancher M., Vitali M., *Controllo e diagnostica di un sistema di prova ingranaggi per applicazioni aeronautiche*, Atti del XXXII Congresso AIAS, Salerno, 3-6 Settembre 2003.
[17] Barbato D., Barsanti M., Mordacci G., Plancher M., Vitali M., *Confronto di tecniche di analisi on-line e off-line per segnali accelerometrici di ingranaggi ad alta velocità*, Atti del XXXIII Congresso AIAS, Bari, 31 Agosto-2 Settembre 2004.
[18] Ozguven H.N., Houser D.R., 1988, *Mathematical models used in gear dynamics – a review*, Journal of Sound and Vibration, 12, 383-411.
[19] Howard I., Jia S., Wang J., 2001. *The dynamic modelling of a spur gear in mesh including friction and a crack*, Mechanical Systems and Signal Processing, ,15(5), 831-853.
[20] Jia S., Howard I., 2006, *Comparison of localised spalling and crack damage from dynamic modelling of spur gear vibrations*, Mechanical Systems and Signal Processing, 20, 332-349.
[21] Zakrajsek, J.J., Townsend, D.P., and Decker, H.D. *An Analysis of Gear Fault Detection Methods as Applied to Pitting Fatigue Failure Data.* Proceedings of the 47th Meeting of the Mechanical Failures Prevention Group. Office of Naval Research, Arlington, VA., 1993, pp. 199-208, (NASA Technical Memorandum 105950).
[22] Zakrajsek, J.J., Handschuh, R.F., and Decker, H.D. *Application of Fault Detection Techniques to Spiral Bevel Gear Fatigue Data.* Proceedings of the 48th Meeting of the Mechanical Failures Prevention Group. Office of Naval Research, Arlington, VA., 1994, pp. 93-104, (NASA Technical Memorandum 106467).
[23] Decker, H.J., Handschuh, R.F., Zakrajsek, J.J.: *An Enhancement to the NA4 Gear Vibration Diagnostic Parameter*. Proceedings of the 18th Annual Meeting of the Vibration Institute, Hershey, PA, 1994, pp. 259 - 268, (NASA Technical Memorandum 106553).
[24] Stewart, R.M. *Some Useful Data Analysis Techniques for Gearbox Diagnostics.* Report MHM/R/10/77, Machine Health Monitoring Group, Institute of Sound and Vibration Research, University of Southampton, July 1977.
[25] Polyshchuk V.V., Choy F.K., Braun M.J., 2002, *Gear fault detection with time-frequency based parameter NP4* Intern. J. of Rotating Machinery 8(1), 57-70.

 Copyright © 2006 by ASME

Downloaded From: https://proceedings.asmedigitalcollection.asme.org on 06/29/2019 Terms of Use: http://www.asme.org/about-asme/terms-of-use